Icarus 257 (2015) 377–386

Contents lists available at ScienceDirect

Icarus

journal homepage: www.elsevier.com/locate/icarus

Variations of the HDO/H_2O ratio in the martian atmosphere and loss of water from Mars

Vladimir A. Krasnopolsky *,[1]

Department of Physics, Catholic University of America, Washington, DC 20064, USA
Moscow Institute of Physics and Technology (PhysTech), Dolgoprudny, Russia

ARTICLE INFO

Article history:
Received 4 March 2015
Revised 17 April 2015
Accepted 20 May 2015
Available online 27 May 2015

Keywords:
Atmospheres, composition
Abundances, atmospheres
Mars
Mars, atmosphere
Atmospheres, evolution

ABSTRACT

Ground-based spatially-resolved high-resolution spectroscopy is currently the only means to observe variations of the HDO/H_2O ratio in the martian atmosphere. These observations are difficult because telluric water exceeds the martian water by two orders of magnitude even at the excellent conditions of NASA IRTF. Our observations of HDO and H_2O at the close wavenumbers of 2722 and 2994 cm^{-1}, respectively, cover six martian seasons in the period from 2007 to 2014. Infrared properties of water ice and dust are rather similar at these wavenumbers, and the HDO and H_2O line equivalent widths are comparable; therefore effects of aerosol absorption and scattering significantly cancel out in the HDO/H_2O ratios. These ratios are rather constant in wide latitude ranges at four observing sessions, in accord with the GCM model by Montmessin et al. (Montmessin, F., Fouchet, T., Forget, F. [2005]. J. Geophys. Res. 110, E03006). Results of two other sessions demonstrate significant deviations from the model predictions and strong correlation between HDO/H_2O and temperature at ~7 km above the surface with correlation coefficients of 0.9. The observed global-mean HDO/H_2O ratio is 4.6 ± 0.7 times the terrestrial ratio, the ratio in vapor released by the north polar cap is 6.2 ± 1.4, and the ratio in the north polar cap ice is 7.1 ± 1.6. Updating the model of isotope fractionation in hydrogen escape by Krasnopolsky and Feldman (Krasnopolsky, V.A., Feldman, P.D. [2001]. Science 294, 1914–1917), 60 m of the global water layer was lost in the last 4 Byr and more than 1200 m could be lost by hydrodynamic escape of H_2 released in the reaction between water and iron. Variations of telluric D/H above Mauna Kea (Hawaii, elevation 4.2 km) are by-products of our observations; D/H varies from 0.4 to 0.9 in nine observations with a mean D/H = 0.67.

1. Introduction

Preferential escape of hydrogen relative to deuterium through the history of Mars resulted in enrichment in the D/H ratio in water. This enrichment is among key values to study evolution of water on Mars. It was discovered by Owen et al. (1988) who observed the HDO lines near 2722 cm^{-1} (3.67 μm) using the Fourier Transform Spectrometer (FTS) at the Canada-France-Hawaii Telescope. The observed HDO/H_2O in the martian water vapor was equal to 5.8 ± 2.6 times that of 1.56×10^{-4} in the Standard Mean Ocean Water (SMOW). Similar values of 5.2 ± 0.2 and 5.5 ± 2 were measured by Bjoraker et al. (1989) and Krasnopolsky et al. (1997) using the FTSs at the Kuiper Airborne Observatory and the Kitt Peak National Observatory, respectively.

Recently in situ observations of the D/H ratio in the martian water vapor was made using the Tunable Laser Spectrometer at the Curiosity rover (Webster et al., 2013). Measurements for the first ~100 days of the rover operation give $D/H = 6 \pm 1$. However, water vapor abundances in the instrument cell were much higher, up to 1%, than those expected in the atmosphere (~100 ppm), and a reason of this enrichment is not well identified. Other Mars-orbiting and landing spacecraft had no capabilities to observe HDO on Mars.

Atomic deuterium in the martian upper atmosphere was detected (Krasnopolsky et al., 1998) using the Goddard High-Resolution Spectrograph at the Hubble Space Telescope. Molecular hydrogen H_2 was later detected at 15 ± 5 ppm on Mars (Krasnopolsky and Feldman, 2001) using the Far Ultraviolet Spectroscopic Explorer. The measured abundances of D and H_2 were significantly smaller than model predictions at that time. H_2 is the most abundant product of the hydrogen chemistry on

* Address: 6100 Westchester Park Dr. #911, College Park, MD 20740, USA.
E-mail address: vlad.krasn@verizon.net

[1] Visiting Astronomer at the Infrared Telescope Facility, which is operated by the University of Hawaii under Cooperative Agreement No. NCC 5-538 with the National Aeronautic and Space Administration, Science Mission Directorate, Planetary Astronomy Program.

http://dx.doi.org/10.1016/j.icarus.2015.05.021
0019-1035/

Mars. It dissociates in the ionosphere and regulates the hydrogen escape. The observed D and H_2 correspond to a depletion of D/H in H_2 relative to that in water by a factor of 2.5 (Krasnopolsky, 2002), which is explained by a smaller HDO photolysis rate (Cheng et al., 1999) and preferential condensation of HDO (Fouchet and Lellouch, 2000).

The D/H ratios mentioned above present to some extent global-mean values. Ground-based spatially-resolved high-resolution spectroscopy is currently the only means to observe variations of HDO/H_2O on Mars. Novak et al. (2002) initiated observations of the HDO lines at 2722 cm^{-1} using the CSHELL spectrograph at the NASA Infrared Telescope Facility (IRTF). The observed variations of HDO/H_2O at $L_S = 67°$ and 221° were published in Fisher et al. (2008). (Solar longitude L_S specifies seasons on Mars with $L_S = 0$ and 180° at vernal and fall equinoxes.) The measured D/H decreases from ~8 at 20°S to ~4 at 60°N at $L_S = 67°$ and increases from ~4 at 60°S to ~8 at 20°N at $L_S = 221°$. Later Novak et al. (2011) observed variations of HDO/H_2O at $L_S = 50°$ with a peak value of ~7 at 20°N decreasing to the north to ~5.5 near 60°N and ~ 4 at 85°N. The decrease to the south was at ~4.5 at 15–40°S and then to ~3.6 at 50°S.

A new and more detailed study of the HDO/H_2O variations (Villanueva et al., 2015) became available after the submission of this paper. The observations were made using the best ground-based high-resolution spectrographs CRIRES at the Very Large Telescope, CSHELL at NASA IRTF, and NIRSPEC at the Keck telescope. Results of four sessions are selected of all observations in 2008–2014 and presented. The observations were made in a mapping mode with 9–11 slit positions at the martian disk. The observed maps cover seasons $L_S = 335°$, 50°, 80°, and 83°. Actually the last two maps were observed with an interval of five days, and the observing session at $L_S = 50°$ is that was partially described in Novak et al. (2011). The map at $L_S = 335°$ is rather symmetric relative to the equator with D/H ≈ 5 between 40°S and 40°N with smaller and much smaller D/H at the middle and high south and north latitudes, respectively. The maps in spring show D/H ≈ 7 in the northern hemisphere and ~3 in the southern hemisphere. The authors conclude that water vapor released by the north polar cap has D/H ≈ 7, ice in the cap has D/H ⩾ 8, and the initial water abundance on Mars was at least 137 m deep.

Variations of the HDO/H_2O ratio were simulated by Montmessin et al. (2005) using a global circulation model by Forget et al. (1999). The model accounts for the hydrogen isotope fractionation in the condensation and sublimation processes on Mars. Here we present our observations of variations of the HDO/H_2O ratio in the martian atmosphere.

2. Observations

We began our observations of HDO and H_2O in 2007 using the CSHELL spectrograph at NASA IRTF. CSHELL (Greene et al., 1993) is a long-slit echelle spectrograph with an InSb detector that is cooled to 30 K. The detector is an array of 256 × 150 pixels, so that a spectral frame includes 150 spectra along the instrument slit of 30 arcs, and each spectrum consists of 256 pixels. The pixel size is $9 \times 10^{-6}\ \nu_0$ in the dispersion direction and 0.2 arcs in the aspect direction. The instrument selects a narrow spectral range of 0.0023 ν_0, where the central wavenumber ν_0 may be chosen in a wide range from 1800 to 9000 cm^{-1} (5.5–1.1 μm, respectively). The instrument spectral resolving power is $\nu/\delta\nu = 40{,}000$.

The IRTF telescope with diameter of 3 m is on the summit of Mauna Kea with elevation of 4.2 km. Spatial resolution of the telescope and spectrograph combination is ~1 arcs. The best astroclimate on Mauna Kea with a mean overhead water of 2 precipitable mm and atmospheric pressure of 0.6 bar is advantageous for the planetary astronomy.

Telluric water exceeds the martian water vapor abundance by two orders of magnitude even at Mauna Kea. Ground-based observations of the martian H_2O and HDO lines require high spectral resolution and significant Doppler shifts relative to the similar telluric lines from geocentric velocity of Mars. Best combinations of high geocentric velocity and angular size of Mars are usually two months before and after Mars oppositions, with typical values of ~15 km s^{-1} and ~10 arcs. A footprint of an individual spectrum is ~140 × 350 km on Mars, and the spatial resolution corresponds to ~700 km.

We placed the instrument slit along the central meridian of Mars and got spectra of Mars, sky foreground, flat field from a continuum source, and dark current. Spectra of Mars cover a third of the spectral frames, the remaining being the sky foreground. The flat field and dark current were measured after the allocated observing time. The time lag between the H_2O and HDO observations was ~15 min that converts to ~3.5° of longitude. This is a third of the spatial resolution element of 1 arcs.

As in the previous observations of the martian HDO, we measured spectra of Mars centered at 2722 cm^{-1}. Most of our H_2O observations were made at $\nu_0 = 2994$ cm^{-1}, while the H_2O line at 3035.784 cm^{-1} was observed in two sessions.

We had eight IRTF sessions to observe HDO/H_2O on Mars. Each session included two six-hour halfnights. Here we present data of the best halfnights in six sessions. Main observing conditions are given in Table 1.

Quality of our retrieval of water on Mars is sensitive to the overhead telluric water abundance. Both H_2O and HDO telluric abundances may be derived from the observed spectra, and these data are shown in Table 1.

3. Data processing

Initial phase of our data processing is to transform the observed spectra of 256 pixels to a uniform wavenumber scale with a step of 0.001 cm^{-1}. At first the observed spectra are corrected for dark current and flat field: the dark current is subtracted from both the observed and flat field spectra. Then their ratio is corrected for bad pixels that are replaced by means of their two neighbors. Next we apply a parabolic fitting of three adjacent pixels that transforms a pixel value into eight sampling points and keeps the sum of these points at the pixel value. This is better for our analysis than the standard parabolic fitting that fixes the middle sampling point at the pixel value.

Then absorption lines are identified and used to establish wavenumber scales in the spectra that are linearly interpolated to the step of 0.001 cm^{-1}. For the Mars angular diameter of 10 arcs, fifty spectra refer to Mars in a spectral frame and ~100 spectra are the sky foreground. This foreground is properly interpolated and subtracted from the Mars spectra. This subtraction removes the terrestrial nightglow and thermal emissions from aerosol and gas species in the overhead air.

Our basic technique is fitting of the observed spectra by synthetic spectra. This technique requires further adjustments to the observed spectrum. Mars reflectivity and the instrument sensitivity may slightly vary with wavenumber within a spectrum, and we apply a parabola (three parameters) to compensate for these variations. Interactions between optical elements of the instrument make a weak variable component in the spectrum that is approximated by a sinusoid and subtracted using three parameters (amplitude, period, and phase). Typically the sinusoid period is ~15 resolution elements in the spectrum, amplitude is ~1%, and its subtraction helps to more accurate fitting of the spectral

Table 1
Conditions of the IRTF/CSHELL observations of the HDO/H_2O ratio on Mars.

Date	2007/10/16	2008/03/09	2009/12/07	2010/03/30	2012/01/22	2012/05/10	2014/02/12	2014/06/04
L_S	330	42	20	70	60	110	89	145
Central latitude	6°N	1.5°N	19°N	14°N	23°N	24°N	20°N	25°N
LT	14:25	09:50	14:10	09:50	14:00	09:20	14:15	09:35
Longitude	15°E	20°E	9°W	36°E	90°W	107°W	57°W	24°W
Diameter, arcs	10.8	8.4	10.4	9.4	10.9	9.2	9.9	11.6
V_g, km/s	−11.2	17.0	−13.0	15.2	−13.2	13.8	−15.8	10.9
V_h, km/s	2.2	1.1	1.75	0.0	0.4	−1.4	−0.7	−2.1
Exposure, min	2	2	12	8	8	12	8	12
H_2O, pr. mm	4.18	1.23	1.96	1.13	1.23	0.924	2.01	3.28
HDO/H_2O	0.916	0.74	0.76	0.545	0.69	0.47	0.75	0.80

V_g, V_h are geocentric and heliocentric velocities of Mars, respectively; H_2O in pr. mm and HDO/H_2O are abundances of the telluric overhead water and its isotope ratios derived from our observations.

continuum. Small errors in wavenumbers result in significant differences between the observed and synthetic spectra. Therefore we apply wavenumber corrections at the edges and in the middle of the observed spectrum. Overall, nine parameters are used to adjust each observed spectrum.

A processed and adjusted spectrum of HDO is shown in Fig. 1. It was observed on May 10, 2012, at $L_S = 110°$ and 43°N. All significant spectral features are the HDO telluric and martian absorption lines.

Synthetic spectra are calculated using the HITRAN 2012 spectroscopic database (Rothman et al., 2013) and the ATMOS high-resolution solar spectrum (Farmer and Norton, 1989) modified by Kurucz (2011, http://kurucz.harvard.edu/sun/atmos/). Telluric water is specified by its abundance, mean temperature and pressure (three parameters). Other parameters are a ratio of the reflected solar to thermal radiation, abundances of telluric methane and martian HDO, and the instrument spectral resolution, that is, seven parameters per a synthetic spectrum.

Lines of telluric methane are weak near 2722 cm^{-1}, and we adopt their mean pressure at half pressure at Mauna Kea and their mean temperature at 225 K, close to that in the standard atmosphere at a level of 300 mbar. The collision broadening profile is applied to calculate the telluric lines.

The martian HDO lines are calculated using the Voigt line shape and data on the collision broadening of H_2O and its isotopologues in CO_2 from Gamache et al. (2011). (These data are very different from those in Gamache et al. (1995).) Pressure and temperature of line formation are set to half of the surface pressure, and the values are taken from the MGS/TES observations (Smith, 2004) for the similar seasons, latitudes and longitudes averaged for three martian years. The martian water is usually assumed to be uniformly mixed in the atmosphere with a steep cutoff at a condensation level. Mean pressures and temperatures of the martian water are therefore greater than those at the half pressure levels. However, our attempts of their further adjustment gave negligible improvements in the HDO/H_2O ratios. We approximate the instrument response function by a Gaussian with a variable width that accounts for small variations of spectral resolution along the spectral frames.

The best-fit telluric spectrum and difference between the observed and synthetic telluric spectrum are shown in Fig. 1. This difference clearly indicates the martian Doppler-shifted HDO lines. Mean difference between the observed spectrum and the full synthetic spectrum that includes the solar, telluric, and martian lines (Fig. 1) is 0.3%. The total number of free parameters of fitting is sixteen and much smaller than the number of degrees of freedom, 256 pixels.

Processing and fitting of the H_2O spectra at 2994 cm^{-1} is similar to those at 2722 cm^{-1} (Fig. 2) except some features. We have made some tests and concluded that thermal radiation of Mars is very much weaker than the reflected sunlight at 2994 cm^{-1} and may

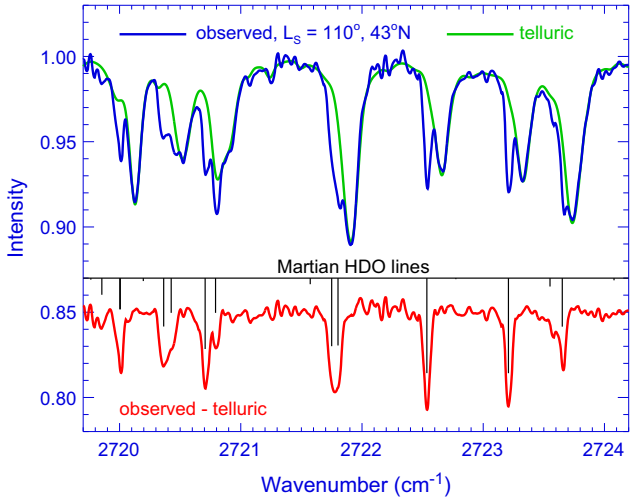

Fig. 1. Processed and adjusted spectrum of HDO is compared with the best fit telluric spectrum. Their difference reveals martian HDO lines; their strengths and Doppler-shifted positions are indicated.

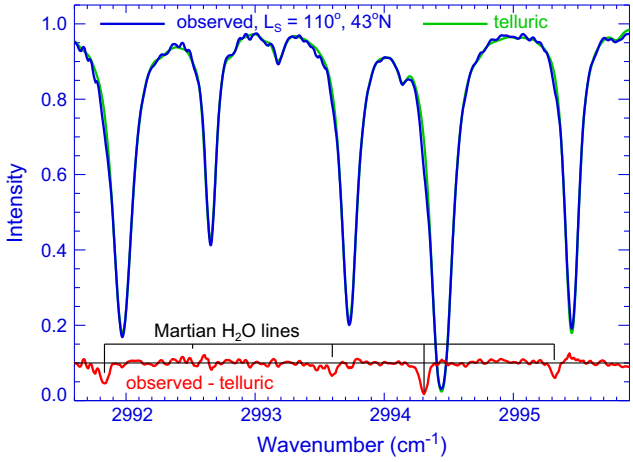

Fig. 2. Processed and adjusted spectrum of H_2O is compared to the best fit telluric spectrum. Their difference reveals martian H_2O lines; their strengths and Doppler-shifted positions are indicated.

be neglected in our analysis. This parameter is replaced by a parameter that describes scattered light in a spectrum. It is subtracted from the observed spectrum, and this improves significantly the spectral fits for the telluric H_2O lines. A typical value of the scattered light is ~4% of the continuum. Next, there are weak telluric O_3 lines and weak martian CO_2 lines in the spectrum. The O_3 lines are calculated assuming the ozone abundance of

0.35 cm-atm. CO_2 abundances, temperatures, and pressures are taken from the MGS/TES data to calculate the CO_2 absorption lines. The number of free parameters for fitting to the observed H_2O spectra is sixteen, similar to that for HDO.

Comparing Figs. 1 and 2, one may conclude that extraction of the martian H_2O abundances from the ground-based spectra at 2994 cm^{-1} is a more difficult task with greater uncertainties than those for HDO. Mean difference between the observed and synthetic H_2O spectra is 0.7%, greater than 0.3% for HDO. The large HDO/H_2O on Mars and a depleted HDO/H_2O above Mauna Kea (see Section 6 below) are favorable for the observations of HDO on Mars, while the observations of H_2O are less advantageous.

The H_2O lines in our spectra near 2994 cm^{-1} have halfwidths in air of ~0.05 cm^{-1} at the standard conditions, while these halfwidths are typically ~0.1 cm^{-1} for the H_2O lines. This fact is favorable for observations of the martian water.

4. Results

Evidently our observations of water vapor on Mars cannot compete with the numerous spacecraft H_2O observations. Our goal is variations of the HDO/H_2O ratio, and we expect that simultaneous observations of both HDO and H_2O by the same instrument at the close wavenumbers that are processed similarly would cancel out some errors for each species in their ratio.

We do not account for effects of the aerosol absorption and scattering in our analysis. Therefore the retrieved water abundances may be underestimated up to a factor of 2 (Villanueva et al., 2015). However, extinctions by dust and water ice aerosol differ between 2722 and 2994 cm^{-1} just by 7% and 18%, respectively (Villanueva et al., 2015). Furthermore, mean HDO line strengths are weaker than those of H_2O by a factor of ~5 near these wavenumbers, so that the mean equivalent widths of the HDO and H_2O absorption lines are rather similar for HDO/$H_2O \approx 5$. Therefore errors associated with the neglect of the aerosol absorption and scattering should be compensated in the HDO/H_2O ratios.

Observing conditions (Table 1) were the best on May 10, 2012: the lowest overhead water of 0.92 pr. mm and the clear sky that made it possible perfect guiding of Mars and comparatively long exposures of 12 min for both H_2O and HDO. Furthermore, water is near the seasonal peak in the northern hemisphere at $L_S = 110°$. The retrieved H_2O abundances are compared in Fig. 3 with the TES and SPICAM (Trokhimovskiy et al., 2015) data at the same season averaged for three and five martian years, respectively. The H_2O distribution from the Mars Climate Database (Navarro et al., 2014) is shown as well.

The TES and MCD data refer to the observed longitude while the SPICAM data are zonal mean. Martian local time in our observations is either ~10:00 or ~14:00 (Table 1). The MCD data in our figures are taken for the local times in our observations. The TES data were measured at 14:00, and the SPICAM results were observed at variable local time near local noon. The differences in local times may contribute to the differences between the observed water abundances.

Uncertainties in Fig. 3 and other figures below reflect random errors associated with the fitting differences discussed above. Some systematic errors from uncertainties of the input data for the synthetic spectra and assumptions in their calculations are not ruled out.

Our data perfectly agree with the TES observations up to 60°N. The difference at the higher latitudes may be attributed to the significant increase in both H_2O abundance and airmass. Optical depth reaches ~4 in the H_2O line centers, and even moderate dust and water ice aerosol may significantly affect the derived water abundances (Villanueva et al., 2015).

The retrieved D/H ratio is constant at 4.3 from the north pole to 20°N and gradually decreasing to ~1 near 50°S. This decrease is steeper than the GCM prediction. Temperature at a level of line formation (that is, at half of the surface pressure) is plotted in the lower panel of Fig. 3 as well. This temperature was taken from the TES data (see Section 3). There is a distinct correlation between D/H and this temperature with correlation coefficient of 0.90.

The sky was clear, guiding of Mars was perfect, and the overhead water was rather low at 1.23 pr. mm on January 22, 2012, when we observed Mars at $L_S = 60°$ (Fig. 4). The retrieved H_2O abundances agree with the SPICAM data southward of 25°N and at 80–90°N, being smaller than the TES, SPICAM, and MCD abundances at 25 to 80°N. The observed D/H ratio (lower panel in Fig. 4) is constant at ~5.7 from 30°S to the north pole, in reasonable agreement with the GCM data.

The telluric water was low at 1.23 pr. mm in our observation on March 9, 2008 at $L_S = 42°$; however, cirrus cloud appeared, guiding was poor, and we chose two-minute exposure frames for retrieval of H_2O and HDO. The results are shown in Fig. 5. The observed H_2O

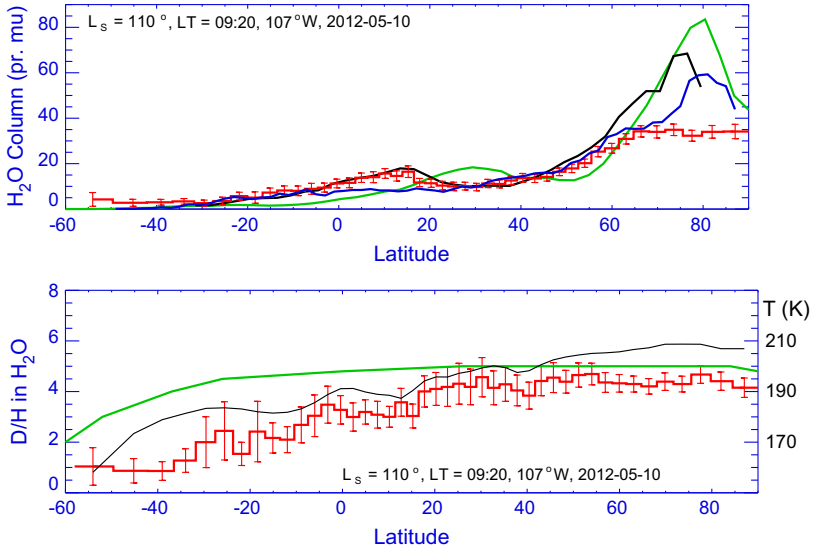

Fig. 3. Observations of H_2O and HDO/H_2O at $L_S = 110°$ (red lines) are compared to the GCM data (green curves), TES (black curve) and SPICAM (blue curve) observations of H_2O. Black curve in the lower panel shows temperatures at the line formation (half surface pressure) level. (For interpretation of the references to color in this figure legend, the reader is referred to the web version of this article.)

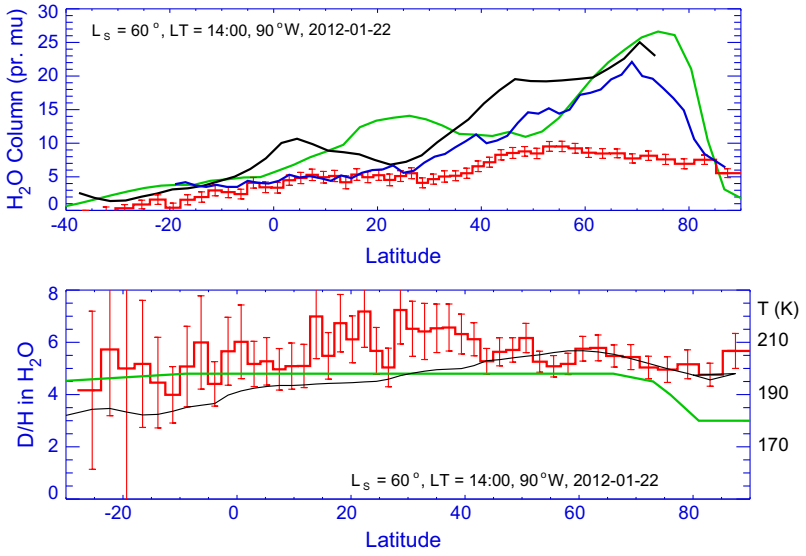

Fig. 4. Observations of H_2O and HDO/H_2O at L_S = 60° (red lines) are compared to the GCM data (green curves), TES (black curve) and SPICAM (blue curve) observations of H_2O. Black curve in the lower panel shows temperature at the line formation (half surface pressure) level. (For interpretation of the references to color in this figure legend, the reader is referred to the web version of this article.)

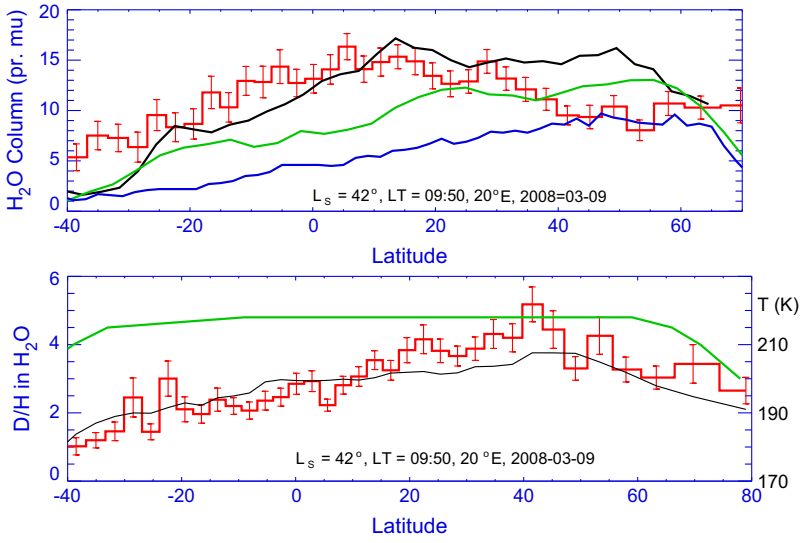

Fig. 5. Observations of H_2O and HDO/H_2O at L_S = 42° (red lines) are compared to the GCM data (green curves), TES (black curve) and SPICAM (blue curve) observations of H_2O. Black curve in the lower panel shows temperature at the line formation (half surface pressure) level. (For interpretation of the references to color in this figure legend, the reader is referred to the web version of this article.)

is in reasonable agreement with the TES measurements, and differences between all four curves in the upper panel in Fig. 5 are comparable. The measured D/H is ~4.3 at 20–55°N decreasing to ~3 at 80°N and ~1 at 40°S. The GCM does not show this trend and gives D/H ≈ 4.7 from 30°S to 60°N. There is a strong correlation of the retrieved D/H with temperature at the level of line formation (Fig. 5), and the correlation coefficient is 0.89.

Our observations on October 16, 2007, February 12, 2014, and June 4, 2014 at L_S = 330°, 89°, and 145° were conducted with the overhead telluric water of 4.18, 2.01, and 3.28 pr mm, respectively. The retrieved H_2O abundances are much smaller than the TES, SPICAM, and MCD data and badly affect the relevant HDO/H_2O ratios. We do not trust those data. The HDO retrievals are more reliable even at the elevated telluric water, and Fig. 6 shows ratios of the observed HDO at L_S = 145° to the TES H_2O at the same season and longitude. These ratios agree with the GCM predictions.

We suspect that Villanueva et al. (2015) met the similar problem of the poor H_2O retrievals at high telluric water, and their presented four sessions are not all observing data collected by them for 2008–2014.

5. Observations using the H_2O line at 3036 cm^{-1}

We had two IRTF sessions when both Mars and the Moon were observed. We developed a technique (Krasnopolsky, 2012) that combines spectra of Mars, Moon, foreground, and the solar spectrum to subtract telluric and solar lines from the martian spectrum and give equivalent widths of martian absorption lines. Then the extracted line equivalent widths are used to retrieve species abundances.

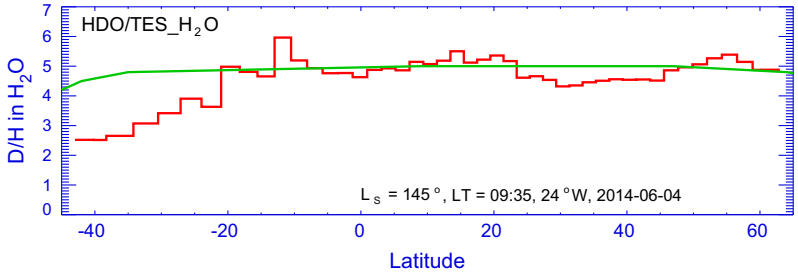

Fig. 6. Ratios of the measured HDO and the TES H_2O observed at the same season and longitude. The GCM predictions (Montmessin et al., 2005) are shown by the green line. (For interpretation of the references to color in this figure legend, the reader is referred to the web version of this article.)

This technique was primarily aimed at improved search for methane on Mars using its R0 and R1 lines. The H_2O line at 3035.784 cm^{-1} is close to the CH_4 R1 line at 3038.498 cm^{-1}, and both lines were observed in the same spectrum. An example of this fitting to the H_2O line from the session on March 30, 2010 is shown in Fig. 7. The observing conditions were excellent, exposure of 8 min, and telluric water was low at 1.13 pr mm.

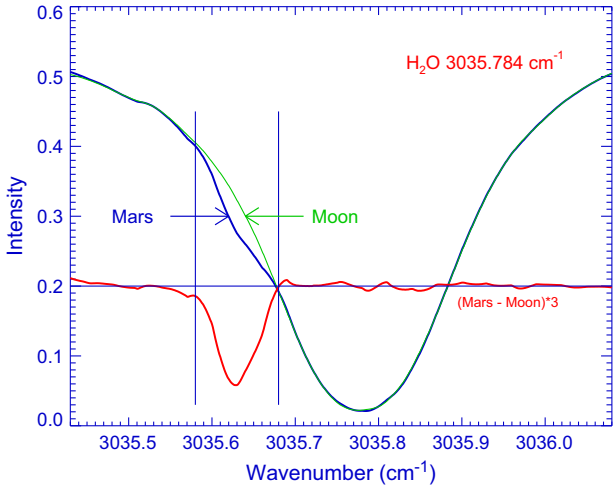

Fig. 7. Subtraction of the Moon spectrum from the Mars spectrum of the H_2O line at 3035.784 cm^{-1} near the equator in the observation on March 30, 2010. Position of the martian Doppler-shifted H_2O line is shown by the vertical lines.

We analyzed the H_2O observational data using both subtraction of the Moon spectra and fitting by synthetic spectra, and the results are exposed in Fig. 8. (The Moon spectra were not applied to the HDO extraction.) The results from both methods are rather similar. The measured H_2O abundances agree with the TES, SPICAM, and MCD data in the southern hemisphere and up to 30°N and smaller than those at the higher northern latitudes. This may be explained by the increasing H_2O and airmass that make significant the effects of aerosol extinction. The measured D/H is almost constant at ~6 from 40°S to the north pole with a decrease to ~3 at 55°S.

Correlation between D/H and temperature at the line formation level in Fig. 8 is not so prominent as those in Figs. 3 and 5 for $L_S = 110°$ and 42°. The correlation coefficient, 0.72, is smaller as well. D/H versus $T(p_0/2)$ for the data from Fig. 8 is depicted in Fig. 9. The solid line is weighted least-square linear fit to the data. This figure is similar to those in Villanueva et al. (2015).

The similar observation on December 7, 2009 is not so good because of the greater telluric water of 1.96 pr mm (Fig. 10). The H_2O retrieval was made by subtraction of the Moon spectra. The measured H_2O abundances are close to the SPICAM data. The mean D/H ratio is rather constant at ~5 from 30°S to 70°N. This behavior and the high-latitude decreases in D/H agree with the GCM

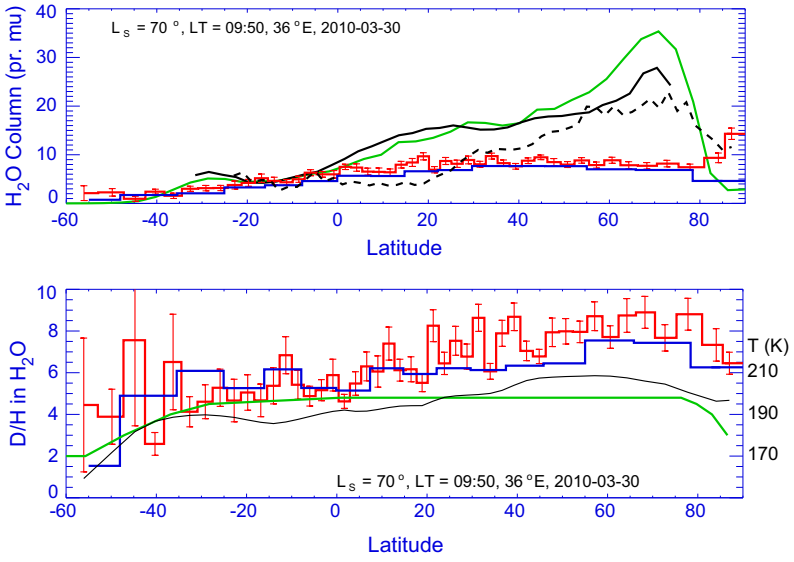

Fig. 8. Abundances of H_2O and D/H ratios retrieved from the observation on March 30, 2010 using fitting by synthetic spectra (red) and subtracting spectra of the Moon for H_2O (blue). The results are compared with the GCM predictions (green) and with the TES and SPICAM observations of H_2O (solid and dashed black curves, respectively). Black curve in the lower panel shows temperature at the line formation (half surface pressure) level. (For interpretation of the references to color in this figure legend, the reader is referred to the web version of this article.)

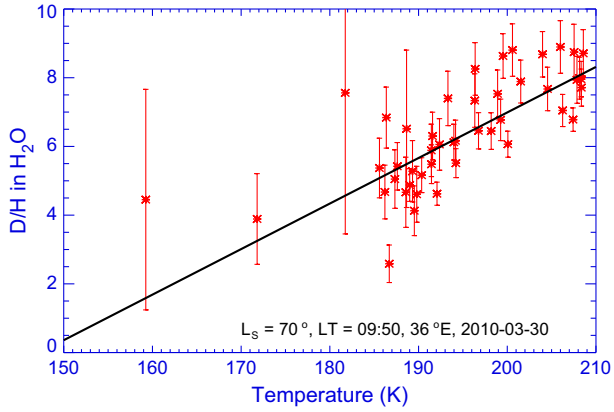

Fig. 9. Correlation between D/H and temperature at the level of line formation for the data in Fig. 8. The black line is the weighted least-square linear fit to the data.

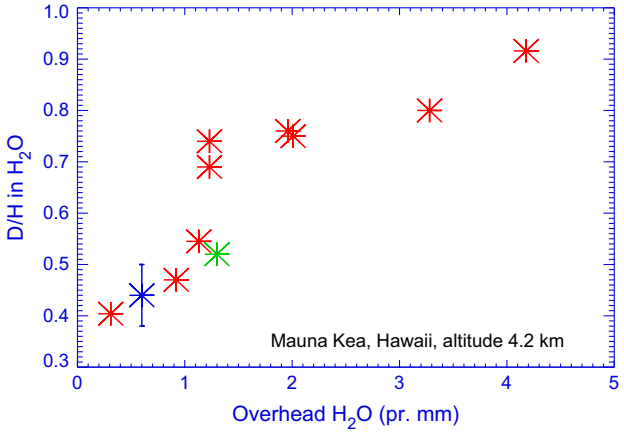

Fig. 11. HDO/H_2O ratio as a function of the water abundance above Mauna Kea. The symbol size is chosen to approximate the data uncertainties. The green symbol is from Villanueva et al. (2012). The blue symbol refers to Mauna Loa, elevation 3.4 km (Rinsland et al., 1988). (For interpretation of the references to color in this figure legend, the reader is referred to the web version of this article.)

predictions. Significant differences between the neighbor values in Fig. 10 reflect large random uncertainties in this observation.

6. Variations of the D/H ratio above Mauna Kea

Telluric abundances of H_2O and HDO are by-products of our observations that are measured with much better uncertainties than those on Mars. The extracted HDO/H_2O ratios in the atmosphere above Mauna Kea (elevation 4.2 km) are shown versus the observed H_2O in Fig. 11. Here we add a point from our observations of Venus on August 18, 2012 (Krasnopolsky et al., 2013).

Variations of the HDO/H_2O ratio were observed in the stratosphere using high-resolution infrared spectroscopy from the ATMOS (Rinsland et al., 1991; Kuang et al., 2003) and ACE (Nassar et al., 2007) orbiters and balloons (Dinelli et al., 1997). With the declining temperature in the troposphere, the H_2O mixing ratio decreases from a few percent at the sea level to a few ppm at the tropopause that acts as a cold trap. The H_2O abundance in the stratosphere is comparable with that of CH_4, and gradual oxidation of methane with preferential oxidation of CH_3D results in a weak growth of both H_2O and HDO/H_2O in the stratosphere. The latter is from ~0.4 near 20 km to ~0.5 at 40 km, and the results of three teams are rather similar in this range. The ATMOS and ACE data extend down to 8 and 10 km at the low latitudes, where mean HDO/H_2O ratios are equal to 0.57 (Kuang et al., 2003) and 0.53 (Nassar et al., 2007), respectively.

Data on HDO/H_2O are scarce in the middle troposphere. A model by Moyer et al. (1996) predicts $HDO/H_2O \approx 0.9$ near 5 km, while our mean value is 0.675, and its variability may be described by standard deviation of 0.167. Fig. 11 includes observations by Villanueva et al. (2012) and Rinsland et al. (1988), the latter at Mauna Loa at elevation of 3.4 km on the same Hawaii Big Island. Three air samples collected in one day during clear sky at Mauna Kea showed H_2O mixing ratios between 800 and 2000 ppm and HDO/H_2O between 0.68 and 0.76 (Galewsky et al., 2007). Evidently the samples at Mauna Kea are not similar to our observations that sound the total overhead atmosphere, though the mean values are rather close. Our observations at nine dates that extend over seven years may significantly complement the existing data.

7. Discussion

The global circulation model for the HDO/H_2O ratio in the martian atmosphere by Montmessin et al. (2005) involved the

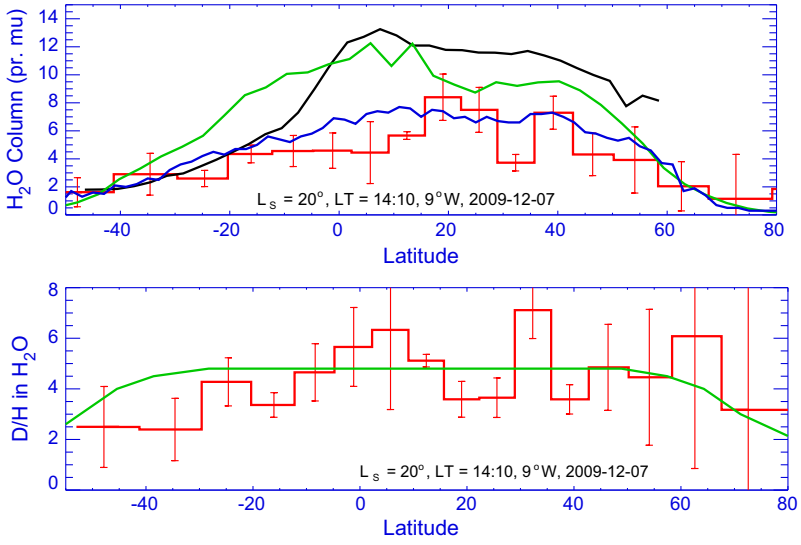

Fig. 10. Observations of H_2O and HDO/H_2O at $L_S = 20°$ (red lines) are compared to the GCM data (green curves) and TES (black curve) and SPICAM (blue curve) observations of H_2O. (For interpretation of the references to color in this figure legend, the reader is referred to the web version of this article.)

atmospheric dynamics and the hydrogen isotope fractionation in condensation and sublimation of water vapor. The model adopts $HDO/H_2O = 1.7 \times 10^{-3} = 5.5$ SMOW in the north polar cap (NPC) that is the main source of the atmospheric water in the model. The model predicts $D/H \approx 4$–5 in all regions where the column H_2O abundance exceeds ~2 pr. μm, and D/H decreasing to the polar regions where temperatures are low and water is freezing out with preferential condensation of HDO.

Montmessin et al. (2005) calculated two models assuming either rapid homogenization or Rayleigh distillation of HDO in the ice aerosol particles, and the results differ just by a few percent. They pointed out two weaknesses of their model: (1) laboratory data by Merlivat and Nief (1967) on the D/H fractionation between water ice and vapor at 230–273 K are extrapolated to the martian temperatures down to 145 K and (2) the model does not account for adsorption and desorption of water vapor by the regolith and possible isotope fractionation in these processes. The residual NPC is a source of water vapor in the model with recycling of water between the cap and the atmosphere, while the residual south polar cap is its permanent sink in the current epoch.

Evidently one may expect significant deviations from the model, and they have been observed at $L_S = 110°$ southward of 20°N (Fig. 3) and at $L_S = 42°$ (Fig. 5). These observations demonstrate the highest correlations between D/H and temperature at the line formation level. According to Merlivat and Nief (1967),

$$\left(\frac{D}{H}\right)_{ice} \Big/ \left(\frac{D}{H}\right)_{vapor} = \exp\left(\frac{16288}{T^2} - 0.0934\right)$$

and low temperatures stimulate depletion of D/H in the H_2O vapor. This explains the observed correlations with coefficients of 0.9 and 0.89 at these seasons, respectively. Four of the six observations, those at $L_S = 60°$, 145°, 70°, and 20° (Figs. 4, 6, 8 and 10), show constant D/H in wide latitude ranges, similar to the GCM predictions.

Seasonally mean D/H ratio may be calculated using

$$\left(\frac{D}{H}\right)_m = \int_{-\pi/2}^{\pi/2} \{HDO\} \cos\varphi \, d\varphi \Big/ \int_{-\pi/2}^{\pi/2} \{H_2O\} \cos\varphi \, d\varphi$$

Here {HDO} and $\{H_2O\}$ are the observed HDO and H_2O column abundances and φ is latitude. Then the mean for six observed seasons is $D/H = 4.6 \pm 0.7$, while the GCM gives the globally and annually mean D/H = 4.8 (based on Fig. 16 in Montmessin et al. (2005)).

The first HDO/H_2O observations by Owen et al. (1988), Bjoraker et al. (1989), and Krasnopolsky et al. (1997) covered significant parts of the martian disk, and the observed $D/H = 5.8 \pm 2.6$, 5.2 ± 0.2, and 5.5 ± 2, respectively, are typically considered as global-mean values. Those observations were made near Mars perihelion at $L_S = 315°$, 245°, and 222°, respectively, while our observations ($L_S = 20°$ to 145°) refer to the aphelion period. This could explain the difference between the data; however, the GCM predicts low seasonal variations of the global HDO/H_2O.

To get D/H in water vapor released from the NPC, we averaged the observations at latitudes of 40–80°N in three seasons with the highest evaporation rate at $L_S = 60°$, 70°, and 110°. Then the released water vapor has $D/H = 6.2 \pm 1.4$, and the ice in the NPC has D/H greater by a factor of ~1.15 according to the GCM, that is, $(D/H)_{ice} = 7.1 \pm 1.6$. This enrichment is between the cases of fast evaporation without isotope fractionation and very slow evaporation with the D/H enrichment in ice by a factor of 1.37 at 200 K using the above formula. The retrieved D/H in water vapor near the NPC and in the NPC ice agree within the uncertainties with the values of ~7 and at least 8, respectively, from Villanueva et al. (2015).

According to Jakosky et al. (1995), a surface ice layer of ~150 μm thick is recycling annually at the NPC. Does the obtained $D/H \approx 7$ refer to the skin layer or to the bulk NPC ice? A fate of the NPC depends on the obliquity and eccentricity variations (Laskar et al., 2004). The obliquity variations have period of ~0.1 Myr and amplitude varying with a period of ~1 Myr. Maximal obliquities reached 35° in the last 3 Myr and 45° between 5 and 20 Myr ago (Laskar et al., 2004). Jakosky et al. (1995) calculated annual sublimation rate of ~3 cm/yr for 35° and ~10 cm/yr for 45°, and the values are uncertain within a factor of 3. Time of the maximum sublimation is ~0.2 of the period, that is, $\sim 2 \times 10^4$ yr. Using the NPC thickness of 2 km, we conclude that the NPC could sublime only partly in the last 3 Myr and almost completely between 5 and 20 Myr ago. Therefore HDO is rather well mixed in the NPC ice and the derived $D/H \approx 7$ refers to the bulk NPC.

8. Loss of water from Mars

Here we will update the estimates by Krasnopolsky and Feldman (2001) and Krasnopolsky (2002). The HST detection of atomic D in the martian upper atmosphere (Krasnopolsky et al., 1998) was compared with the existed model data on H_2 to give a low value of 0.02 for the hydrogen escape isotope fractionation factor (hereafter fractionation factor)

$$F = \frac{\Phi_D/\Phi_H}{D/H}$$

where Φ_i is the escape flux of species i. Later the FUSE detection of H_2 in the martian upper atmosphere (Krasnopolsky and Feldman, 2001) showed a smaller abundance of H_2 (17 ppm) than the model data. That was coupled with a significant deuterium fractionation in photolysis of H_2O (Cheng et al., 1999) and in condensation of water (Fouchet and Lellouch, 2000) to yield $F = 0.105$ (Krasnopolsky, 2002) averaged over the solar activity cycle.

To model isotope fractionation in hydrogen escape on Mars, Krasnopolsky (2000) proposed a scheme with three reservoirs of water: (1) the bulk water with an initial $(D/H)_0$, (2) water in the permanent polar caps, and (3) water in the atmosphere and in the seasonal polar caps. Reservoirs (2) and (3) have D/H ratios that are determined by the fractionation in the sublimation/condensation processes. Hydrogen escapes from (3) and is replenished from (2), and (2) is supplied from (1). Differential equations for H and D in this system give a solution

$$r(t) = \frac{1}{F} - \left(\frac{1}{F} - 1\right) e^{-\alpha(t)F}$$

Here $r = (D/H)/(D/H)_0$ and α is the ratio of total loss of water to its initial abundance in reservoir (2). The solution may be rewritten as

$$\alpha = \frac{1}{F} ln \frac{1 - F}{1 - Fr}$$

Krasnopolsky and Feldman (2001) divided the water history in two periods before and after the first 0.3–0.5 Byr. $(D/H)_0$ was equal at that time to 1.9 in Leshin (2000) and 2.2–4 in Kurokawa et al. (2014); we will use $(D/H)_0 = 2.2$ to combine with the derived current $D/H \approx 7$ in the NPC. This gives $r = 3.2$ and $\alpha = 2.8$. Amounts of water ice in the NPC and the south layered deposits are 10 m (Zuber et al., 1998) and 11 m (Plaut et al., 2007) of global equivalent layer, respectively. Then the lost water is $2.8 \times 21 \approx 60$ m for the last ~4 Byr, and the total water exceeded 80 m ~4 Byr ago.

There are some evidences, including abundances and isotope ratios of the noble gases, for hydrodynamic escape from the early Mars. Hydrodynamic escape of water is only possible for comparable abundances of H_2O and CO_2 in the atmosphere (Kasting and Pollack, 1983), and a liquid water ocean is insufficient to drive hydrodynamic escape on Mars. More probable is hydrodynamic escape of H_2 released by

$$Fe + H_2O \rightarrow FeO + H_2$$

from the hot Mars after the accretion. Fractionation factor for this escape is $F_h = 0.8$ (Zahnle et al., 1990), $(D/H)_0 = 1.275$ according to Kurokawa et al. (2014), the final $D/H \approx 2.2$, and the final water abundance is more than 80 m. Then an initial water abundance is more than

$$80 \times (2.2/1.275)^{1/(1-0.8)} = 1200 \text{ m}.$$

This abundance is similar to that obtained by Krasnopolsky and Feldman (2001), and some changes in the initial data are compensating. The terrestrial water ocean scaled to the Mars size and mass is 1 km deep, and the calculation confirmed a conclusion by Dreibus and Waenke (1987) that Mars was initially even richer in water than Earth. Supply of water by cometary impacts is much smaller than the above estimates and cannot affect them (Krasnopolsky, 2002).

Escape of hydrogen is balanced by nonthermal escape of oxygen and its loss in oxidation of the surface rocks.

9. Conclusions

Ground-based spatially-resolved high-resolution spectroscopy is currently the only means to observe variations of the HDO/H_2O ratio in the martian atmosphere. These observations are difficult because telluric water exceeds the martian water by two orders of magnitude even at the excellent conditions of NASA IRTF. Our observations of HDO and H_2O at the close wavenumbers of 2722 and 2994 cm^{-1}, respectively, cover eight martian seasons in the period from 2007 to 2014. The extracted martian H_2O becomes rather uncertain if the overhead telluric water exceeds 2 pr mm, and the data of two sessions are of low quality and not discussed here.

Infrared properties of water ice and dust are rather similar at the chosen wavenumbers, and the HDO and H_2O line equivalent widths are comparable; therefore effects of aerosol absorption and scattering significantly cancel out in the HDO/H_2O ratios. This makes it possible to avoid corrections for aerosol extinction in our code.

The HDO/H_2O ratios are rather constant in wide latitude ranges at four observing sessions, in accord with the GCM model by Montmessin et al. (2005). Results of two sessions demonstrate significant deviations from the model predictions and strong correlation between HDO/H_2O and temperature at ~7 km above the surface with correlation coefficients of 0.9. This agrees with the temperature dependence of HDO/H_2O fractionation between water vapor and ice.

The observed global-mean HDO/H_2O ratio is 4.6 ± 0.7 times the terrestrial ratio, the ratio in vapor released by the north polar cap is 6.2 ± 1.4, and the ratio in the north polar cap ice is 7.1 ± 1.6. Updating the model of isotope fractionation in hydrogen escape by Krasnopolsky and Feldman (2001), 60 m of the global water layer was lost in the last 4 Byr and more than 1200 m could be lost by hydrodynamic escape of H_2 released in the reaction between water and iron.

Variations of telluric D/H above Mauna Kea (Hawaii, elevation 4.2 km) are by-products of our observations. The observed D/H varied from 0.4 to 0.9 with a mean value of 0.67; the measured variations may be described by a standard deviation of 0.17. These results significantly complement the existing data on D/H in the Earth's middle troposphere.

Acknowledgments

This work is supported by NASA Planetary Astronomy Program (Grant NNX12AG28G to V.A. Krasnopolsky) and by Grant 11.G34.31.0074 of the Russian Government to Moscow Institute of Physics and Technology (PhysTech) and V.A. Krasnopolsky. The author is grateful to the IRTF staff for cooperation and support.

References

Bjoraker, G.L., Mumma, M.J., Larson, H.P., 1989. Isotopic abundance ratios for hydrogen and oxygen in the martian atmosphere. Bull. Am. Astron. Soc. 21, 991 (abstract).
Cheng, B.M. et al., 1999. Photo-induced fractionation of water isotopomers in the martian atmosphere. Geophys. Res. Lett. 26, 3657–3660.
Dinelli, B.M. et al., 1997. Geophys. Res. Lett. 24, 2003–2006.
Dreibus, G., Waenke, H., 1987. Volatiles on Earth and Mars – A comparison. Icarus 71, 225–240.
Farmer, C.B., Norton, R.H., 1989. A high-resolution atlas of the infrared spectrum of the Sun and the Earth atmosphere from space. 1. The Sun. NASA Ref. Publication 1224, vol. 1.
Fisher, D., Novak, R., Mumma, M.J., 2008. D/H ratio during the northern polar summer and what the Phoenix mission might measure. J. Geophys. Res. 113, E00A15.
Forget, F. et al., 1999. Improved general circulation models of the martian atmosphere from the surface to above 80 km. J. Geophys. Res. 104, 24155–24175.
Fouchet, T., Lellouch, E., 2000. Vapor pressure isotope fractionation effects in planetary atmospheres: Application to deuterium. Icarus 144, 114–123.
Galewsky, J., Strong, M., Sharp, Z.D., 2007. Measurements of water vapor D/H ratios from Mauna Kea, Hawaii, and implications for subtropical humidity dynamics. Geophys. Res. Lett. 34, L22808.
Gamache, R.R. et al., 1995. CO_2 broadening of water vapor lines. J. Mol. Spectrosc. 170, 131–151.
Gamache, R.R., Laraia, A.L., Lamouroux, J., 2011. Half-widths, their temperature dependence, and line shifts for the HDO–CO_2 collision system for applications to CO_2-rich planetary atmospheres. Icarus 213, 720–730.
Greene, T.P. et al., 1993. CSHELL: A high spectral resolution 1-5-μm cryogenic echelle spectrograph for the IRTF. Proc. SPIE 1946, 313–323.
Jakosky, B.M., Henderson, B.G., Mellon, M.T., 1995. Chaotic obliquity and the nature of the martian climate. J. Geophys. Res. 100, 1579–1584.
Kasting, J.F., Pollack, J.B., 1983. Loss of water from Venus. I. Hydrodynamic escape of hydrogen. Icarus 53, 479–508.
Krasnopolsky, V.A., 2000. On the deuterium abundance on Mars and some related problems. Icarus 148, 597–602.
Krasnopolsky, V.A., 2002. Mars' upper atmosphere and ionosphere at low, medium, and high solar activities: Implications for loss of water. J. Geophys. Res. 107 (E12), 5128.
Krasnopolsky, V.A., 2012. Search for methane and upper limits to ethane and SO_2 on Mars. Icarus 217, 144–152.
Krasnopolsky, V.A., Feldman, P.D., 2001. Detection of molecular hydrogen in the atmosphere of Mars. Science 294, 1914–1917.
Krasnopolsky, V.A. et al., 1997. High-resolution spectroscopy of Mars at 3.7 and 8 μm: A sensitive search for H_2O_2, H_2CO, HCl, and CH_4, and detection of HDO. J. Geophys. Res. 102, 6525–6534.
Krasnopolsky, V.A., Mumma, M.J., Gladstone, G.R., 1998. Detection of atomic deuterium in the upper atmosphere of Mars. Science 280, 1576–1580.
Krasnopolsky, V.A. et al., 2013. Observations of D/H ratios in H_2O, HCl, and HF on Venus and new DCl and DF line strengths. Icarus 224, 57–65.
Kuang, Z. et al., 2003. Measured HDO/H_2O ratios across the tropical tropopause. Geophys. Res. Lett. 30 (7), 1372.
Kurokawa, H. et al., 2014. Evolution of water reservoirs on Mars: Constraints from hydrogen isotopes in martian meteorites. Earth Planet. Sci. Lett. 394, 179–185.
Laskar, J. et al., 2004. Long term evolution and chaotic diffusion of the insolation quantities of Mars. Icarus 170, 343–364.
Leshin, L.A., 2000. Insights into martian water reservoirs from analyses of martian meteorite QUE94201. Geophys. Res. Lett. 27, 2017–2020.
Merlivat, L., Nief, G., 1967. Fractionnement isotopique lors des changements d'etats solide-vapeur et liquide-vapeur de l'eau a des temperatures inferieures a 0°C. Tellus 19, 122–127.
Montmessin, F., Fouchet, T., Forget, F., 2005. Modeling the annual cycle of HDO in the martian atmosphere. J. Geophys. Res. 110, E03006.
Moyer, E.J. et al., 1996. ATMOS stratospheric deuterated water and implications for troposphere–stratosphere transport. Geophys. Res. Lett. 23, 2385–2388.
Nassar, R. et al., 2007. Variability in HDO/H_2O abundance ratios in the tropical tropopause layer. J. Geophys. Res. 112, D21305.
Navarro, T. et al., 2014. Global climate modeling of the martian water cycle with improved microphysics and radiatively active water ice clouds. J. Geophys. Res. 119, 1479–1495.
Novak, R.E. et al., 2002. Mapping of ozone and water in the atmosphere of Mars near the 1997 aphelion. Icarus 158, 14–23.
Novak, R.E., Mumma, M.J., Villanueva, G.L., 2011. Measurement of the isotopic signatures of water on Mars: Implications for studying methane. Planet. Space Sci. 59, 163–168.
Owen, T. et al., 1988. Deuterium on Mars: The abundance of HDO and the value of D=H. Science 240, 1767–1771.
Plaut, J.J. et al., 2007. Subsurface radar sounding of the south polar layered deposits of Mars. Science 316, 92–95.

Rinsland, C.P. et al., 1988. Infrared measurements of atmospheric gases above Mauna Loa, Hawaii, in February 1987. J. Geophys. Res. 93, 12607–12626.
Rinsland, C.P. et al., 1991. Stratospheric profiles of heavy water isotopes and CH_3D from analysis of the ATMOS Spacelab 3 infrared solar spectra. J. Geophys. Res. 96, 1057–1070.
Rothman, L.S. et al., 2013. The HITRAN 2012 molecular spectroscopic database. J. Quant. Spectrosc. Radiat. Trans. 130, 4–50.
Smith, M.D., 2004. Interannual variability in TES atmospheric observations of Mars during 1999–2003. Icarus 167, 148–165.
Trokhimovskiy, A. et al., 2015. Mars' water vapor mapping by the SPICAM IR spectrometer: Five martian years of observations. Icarus 251, 50–64.
Villanueva, G.L. et al., 2012. Water in planetary and cometary atmospheres: H_2O/HDO transmittance and fluorescence models. J. Quant. Spectrosc. Radiat. Trans. 113, 202–220.
Villanueva, G.L. et al., 2015. Strong water isotopic anomalies in the martian atmosphere: Probing current and ancient reservoirs. Science. http://dx.doi.org/10.1126/science.aaa3630 (Supplementary Materials science.aaa3630/DC1).
Webster, C.R. et al., 2013. Isotope ratios of H, C, and O in CO_2 and H_2O of the martian atmosphere. Science 341, 260–263.
Zahnle, K., Kasting, J.F., Pollack, J.B., 1990. Mass fractionation of noble gases in diffusion-limited hydrodynamic hydrogen escape. Icarus 84, 502–527.
Zuber, M.T. et al., 1998. Observations of the north polar cap of Mars from the Mars orbiter laser altimeter. Science 282, 2053–2060.